Rectify Effect of Pedot:PSS/WS_2 Heterostructure

Ka Ho Chan, Sheung Mei Ng, Hon Fai Wong, Chi Wah Leung, Chee Leung Mak*

Department of Applied PhysicsThe Hong Kong Polytechnic University, Hung Hom, Kowloon, Hong Kong, People's Republic of China

*E-mail: apaclmak@polyu.edu.hk

Abstract

Recently, devices based on organic and two-dimensional (2D) materials have been recognized as the easiest way to fabricate hybrid 2D van der Waals (vdW) heterojunction devices for electronic and optoelectronic applications. Depositing organic materials on 2D materials is typically demonstrated by thermal evaporation using high voltage and vacuum systems. In this paper, a simple way to fabricate organic/n-2D heterostructures, where Pedot:PSS is chosen to be the organic material due to its high conductivity, excellent film forming ability and good stability, while WS_2 is selected as the n-2D material due to its well-known properties has been presented. By systematically studying the gate dependent and temperature-dependent *I*–*V* characteristics of the Pedot:PSS/WS_2 heterojunctions, it is demonstrated that the device shows a diode-like behavior with rectification ratio (RF) of ≈5 and a turn on voltage of ≈2 V at room temperature (RT). Furthermore, the rectification ratio of the junction reaches up to 10^3 using a back-gate bias voltage (V_{gs}) of 20 V together with drain–source voltage (V_{ds}) ranging from −4 to 4 V. On the basis of the results, it is demonstrated that this simple technique of fabricating organic/2D vdW heterojunctions can extend to other organics and 2D materials.

Keywords

2-D heterjunction, Pedot:PSS, WS2

1 Introduction

The successful isolation of graphene in 2004[1] has stimulated a lot of interest in exploring the feasibility for applying graphene in electronic devices. Unfortunately, graphene lacks a bandgap,[2] and this limits its applications in electronics and optoelectronics. Besides graphene, other 2D materials, such as transition-metal dichalcogenides (TMDs), MXenes, and others, also exhibit many interesting properties when they are scaled down from bulk to nanoscale.[3] Among 2D materials, TMDs have been intensely studied because of their high carrier mobility, direct–indirect bandgap transition, strong spin–orbit coupling, and good chemical stability.[4] These advantages make TMDs turn into materials suitable for next-generation flexible nano-electronics and nano-optoelectronics applications.[5, 6] TMDs usually is described by formula MX_2, where *M* stands for transition metal (Mo, W, Nb, Ta) and *X* stands for chalcogenide atom (S, Se, Te).[7] WS_2 is one of the representatives of TMDs and has a lot of excellent electrical properties. Monolayer WS_2 is a n-type 2D semiconductor, exhibiting a direct bandgap of 2.0 eV,[8] the highest theoretical mobility of 1000 $cm^2 V^{-1} S^{-1}$ among the semiconducting 2D TMDs due to its reduced effective mass, and a transistor switching ON/OFF ratio of $\approx 10^6$.[9] It is air and chemical stable which is necessary in electronic and optoelectronic device applications and can be used to combine with other materials to construct 2D vdW hybrid heterostructures. Conducting polymers are one of the suitable materials to combine with 2D TMDs to form a 2D vdW heterojunction. A significant advantage of employing conducting polymers in vdW heterojunctions is due to their simple deposition process compared with traditional oxide semiconductors. Furthermore, conducting polymers offer the advantages of low cost and flexibility.[10] A hole transporting poly(3,4-ethylenedioxythiophene) doped with poly styrene-sulfonic acid (Pedot:PSS) is commercially available and often used to be a hole transporting layer in organic solar cells.[11] In

this paper, by using simple spin-coating technique, PEDOT-PSS was easily deposited on WS_2 to form a hybrid organic/inorganic Schottky diode. The turn on voltage of this diode was ≈2 V and the rectification ratio was ≈5. The rectification ratio of the junction was further increased to 10^3 using a back-gate bias voltage (V_{gs}) of 20 V together with drain–source voltage (V_{ds}) ranging from −4 to 4 V. As a result, we have successfully demonstrated that this simple technique introduced in our fabrication of organic/2D van der Waals heterojunction could extend to include other organics and 2D materials.

2 Device Fabrication

The fabrication process of the Pedot:PSS/WS_2 hetero-junction are summarized in Figure **1**. Firstly, mono-layer WS_2 flakes were grown on sapphire substrates using chemical vapor deposition (CVD). Then the flakes were transferred by PMMA wet transfer technique**12** onto p-doped silicon substrates containing a 300 nm SiO_2 layer. Secondly, Au(50 nm)/Ti(5 nm) electrodes were deposited on WS_2 and SiO_2 using e-beam lithography. Here, two electrodes were deposited partially on top of WS_2 and partial on SiO_2, and another two electrodes were totally on SiO_2 near WS_2. PMMA was spin-coated on the whole device. Another e-beam lithography step was used to remove the PMMA (as shown in Figure **1**) in order to open a window to allow the Pedot:PSS depositing onto WS_2 to produce a hetero-junction. Before spin-coating at 2500 rpm into the PMMA window, the Pedot:PSS aqueous solution (Al 4083) was filtered through a 0.45 μm syringe filter. The Pedot:PSS(Al 4083) was purchased from Ossila and the ratio of Pedot:PSS (Al 4083) used was 1:6 which is one of the most commonly used formulations in thin film electronic devices.**13** The device was then thermal annealed on a hot plate at 150 °C for 10 min to enhance the crystallinity of Pedot:PSS. As shown in Figure **1**, our device consists of WS_2 field effect transistor (FET), Pedot:PSS/WS_2 heterojunction, and a Pedot:PSS FET by

selecting different combination of electrodes, which were electrically characterized independently.

3 Materials Characterization

Figure **2**(a) is the optical microscopic image showing the surface morphology of the CVD grown triangle WS_2 on SiO_2/Si after transferring from sapphire. Figure **2**(b) and (c) are the Raman and photoluminescence (PL) spectra of the WS_2 flake, respectively. The Raman peak difference between the A_{1g} mode and E^1_{2g} mode is $61.0\ cm^{-1}$, confirming the presence as well as the monolayer nature of the WS_2.**14** The strong PL peak at the 630 nm (2.0 eV) is responding to the direct bandgap of WS_2. Figure **2**(d) shows the Raman spectrum of Pedot:PSS after depositing on the WS_2 and annealing. The measured spectrum is the same as the standard spectrum of Pedot:PSS, indicating that Pedot:PSS has excellent quality and no degrading or contamination after the deposition as well as thermal annealing.

In this paper, 10 Pedot:PSS/WS_2 devices of similar configuration have been fabricated and characterized, and all the devices showed similar structural and electronic properties. In the following, a typical device has been selected to show their measured electric properties. The characterization was measured under vacuum and dark environments to avoid any unwanted interference.

4 Results and Discussion

The *I*–*V* characteristics of Pedot:PSS films and WS_2 films are shown in Figure **3**. Figure **3**(a) shows the drain–source current (I_{ds}) versus drain–source voltage (V_{ds}) of WS_2 FET for various back gate bias voltage (V_{gs}) taken under vacuum. WS_2 is a n-type semiconductor and its conductivity is expected to exponentially increase when positive back-gate voltage bias is

applied. The rectification ratio of WS_2 FET was about 10^5 which is comparable with literature reported.**9** The non-linear output characteristics of WS_2 FET suggest the existence of Schottky barrier in our FET device with Au/Ti electrodes. Figure **3**(b) shows the transfer characteristic of WS_2 FET. The low OFF state current (10^{-12} A at $V_{ds} = +4$ V) is reached due to the relatively large bandgap and ultrathin nature of monolayer WS_2. Figure **3**(c) shows the current–voltage characteristics of Pedot:PSS film. When the Pedot:PSS was connected in a FET configuration, the slope of the *I–V* curve was linear and did not change with the applied back-gate voltage bias. This behavior is due to the high charge carrier density of the conducting polymer, external electric field should have been screened on the atomic scale, so it follows the ohmic conductor at low voltage bias. Figure **3**(d) shows the optical image of actual Pedot:PSS/WS_2 heterojunction device in order to compare with the device schematic.

Figure **4**(a) shows the drain current–voltage characteristics of the Pedot:PSS/WS_2 heterojunction Schottky diode at various gate voltages in dark and RT conditions. The rectification ratio at $V_{ds} = \pm 4$ V was ≈5 and the device turns on voltages under various back-gate voltage bias was observed to be around 2 V. The *I–V* characteristics of the Pedot:PSS/WS_2 heterojunction were also investigated with various back-gate voltage bias and temperature conditions. Using the back-gate bias voltage, the carrier density in WS_2 could be tuned, and therefore the barrier height of the heterojunction was changed. Compared to Figure **3**(a), it is noticed that Figure **4**(a) clearly shows a rectify effect and the device performance can be tuned by applying different back-gate voltage bias. When the back-gate voltage bias increased from +10 to +30 V, the OFF-state current remained at around 10^{-13} A and the ON-state current increase slightly from around 10^{-11} to 10^{-10} A. However, when the back-gate voltage bias increased from +30 to +50 V, the OFF state current increased from 1.2×10^{-13} A to 3.1×10^{-12} A, but the ON state current was kept at around 10^{-10} A. As a result, the RF ratio increased when gate voltage bias increased from +10 to +30 V but decreased when gate voltage bias increased from +30 to +50 V. Figure **4**(b) plots the variation of

rectification ratio of Pedot:PSS/WS_2 device measured at different drain–source voltage at various back-gate voltages. Drain–source voltage from ±1 to ±4 V also shows a similar trend that the RF ratio increased from 0 to +30 V but decreased from +30 to +50 V. A remarkable RF ratio about 10^3 was reached at $V_{ds} = \pm 4$ V with back-gate voltage bias between +20 and +30 V. These results are comparable with the reported value in other 2D vdW heterostructure devices.**15**-**19** Under +30 V back-gate voltage bias and ±4 V drain–source voltage bias, we noticed that the device has a very low dark current of ≈0.12 pA at the −4 V reverse voltage bias and exponentially increased with forward voltage bias, the maximum measured rectification ratio was about $\approx 10^3$.

Figure **5**(a)–(d) show the drain–source current versus drain–source voltage (I_{ds} vs. V_{ds}) curves as a function of back-gate voltage (V_{gs}) measured at 100, 150, 200, and 250 K, respectively. From the figures, we noticed that the device showed a diode-like behavior at all temperatures. Furthermore, a similar trend that RF ratio reached its maximum at $V_{gs} = 20$ V was also observed at all temperatures. Among different temperatures, the highest RF ratio of 4×10^4 was obtained at 200 K with $V_{gs} = 20$ V, and V_{ds} from −4 to 4 V. However, a relative low RF ratio was observed at RT, which was owing to the large $I_{reverse}$ obtained at RT (as shown in Figure **4**(a)).

The turn on voltage of the diode at various back-gate voltage bias ranging from +20 to +50 V under different temperatures is shown in Figure **6**(a). It was noticed that the turn on voltage of the diode is increased with decreasing back-gate voltage bias and temperature. Given that the Pedot:PSS did not show a field effect but WS_2 did (as demonstrated in Figure **3**), the back gating effect is simply explained as the resistance of WS_2 in our device was changed by the back-gate voltage bias, leading to the variation of the diode current.

The current flow through a Schottky contact can be described by the thermionic emission theory, and the *I*–*V* relationship of a Schottky diode is given by 20

$$I = I_s \exp\left(\frac{qV}{nkT}\right)\left[1 - \exp\left(-\frac{qV}{kT}\right)\right] \quad (1)$$

where

$$I_s = AA^{**}T^2 \exp\left(-\frac{q\varphi}{kT}\right) \quad (2)$$

Here I_s is the saturation current, q is the electron charge, V is the applied voltage, T is the absolute temperature, n is the ideality factor, k is the Boltzmann's constant, A is the contact area, A^{**} is the effective Richardson constant (120 cm^{-2} K^{-2} for n-WS_2),21 and φ is the Schottky barrier height. The effective constant A^{**} is known and the I–V measurement was made to determine the saturation current I_s. Thus, the barrier height can be deduced in terms of the thermionic emission theory.

$$\varphi = \frac{kT}{q}\ln\left(AA^{**}\frac{T^2}{I_s}\right) \quad (3)$$

By Equation **3**,**21** the calculated values of φ is plotted as a function of back-gate voltage bias at room temperature. It is observed that the barrier height of the Schottky diode is strongly depending on the applied back-gate voltage bias. As can be seen in Figure **6**(b), the barrier height was found to decrease with increasing positive back-gate voltage bias.

On the basis of literature**21** and our results, it was noticed that the Schottky junction was formed by Pedot:PSS and WS_2 at all temperatures. Pedot:PSS is a conducting polymer and does not show field effect (in this case, it can be seen as a metal) and WS_2 is a n-type semiconductor. When these two materials are in contact, the Fermi level of the two materials must match at the heterojunction. Figure **7** shows the band diagram after connecting Pedot:PSS and WS_2 in thermal equilibrium. The barrier height depends on the work function of Pedot:PSS and the surface states

on WS_2.**22** When positive gate voltage was applied, the charge density of n-type WS_2 increased from $V_{gs} = 0$ V to $V_{gs} = 50$ V which causes the upward shift of Fermi level in n-type WS_2. The upward shift of Fermi level in n-type WS_2 resulted in a lowering of Schottky barrier which allowed more electrons diffuse toward the Pedot:PSS, thus $I_{forward}$ increased. Due to the thermal activation at high temperature, the charge density of WS_2 was increased significantly that also produced the upward shift of Fermi level, resulting in a lower potential barrier. For temperatures between 100 and 250 K, due to the inhibition of the thermal activation at low temperatures, the charge density was reduced and became the limiting factor of $I_{forward}$.

5 Conclusion

In summary, a gate-tunable Pedot:PSS – monolayer WS_2 van der Waals heterojunction – Schottky diode was demonstrated. With acceptable operating back-gate voltage bias, the device showed a large RF ratio up to 10^3. Under the temperature range of 150 K to room temperature, the device worked well with the rectification ratio increased from 10^3 to 10^4. Compared with other vdW heterojunction systems, p-organic polymer offers the advantages of low cost, flexibility, and transparency, which may facilitate the design of future opto-electronic devices.

Acknowledgment

This work was supported by a research grant of The Hong Kong Polytechnic University (PolyU GUA5G and 1-ZVGH).

Conflict of Interest

The authors declare no conflict of interest.

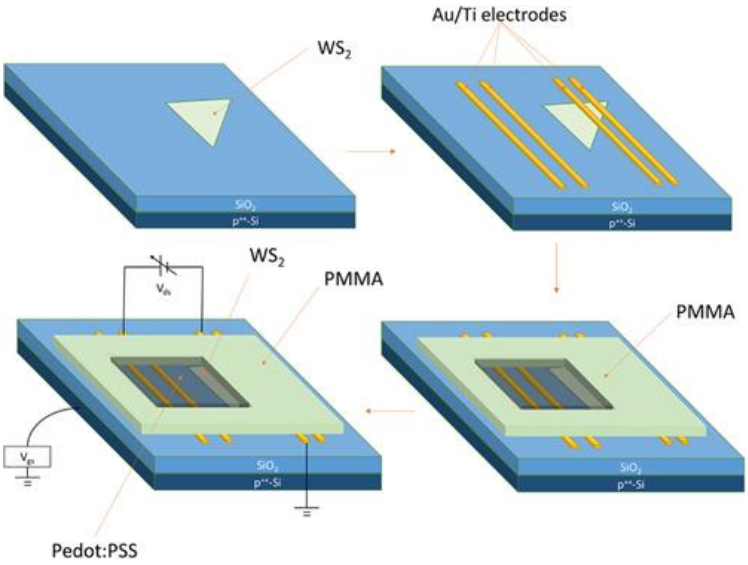

Figure 1. Fabrication procedures of the Pedot:PSS/WS_2 heterojunction devices.

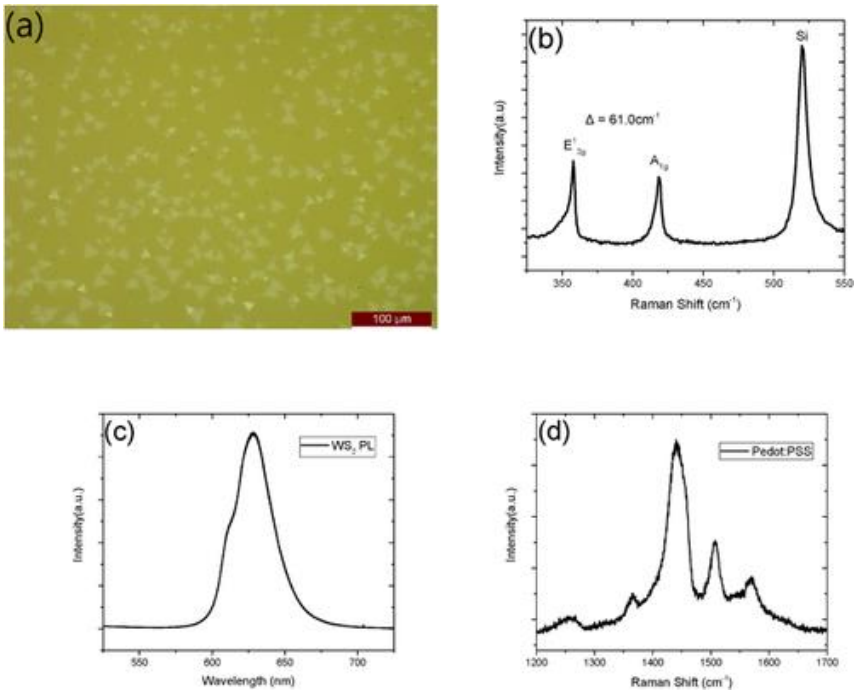

Figure 2. a) Surface morphology of a typical CVD grown triangle monolayer WS_2. b) The Raman spectrum of the CVD grown WS_2. c) The photoluminescence spectrum of the CVD grown monolayer WS_2. The excitation laser is 488 nm. d) The Raman spectrum of Pedot:PSS. The excitation laser is 488 nm.

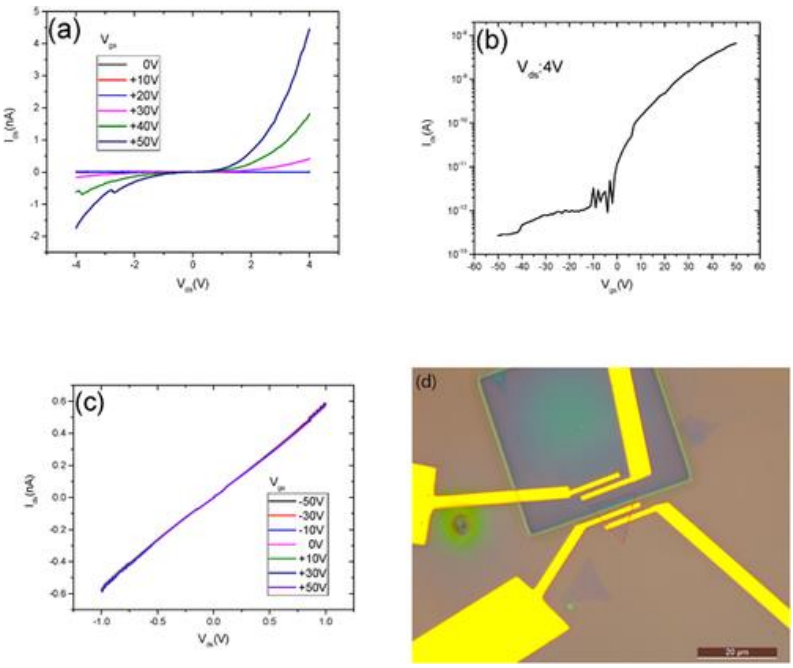

Figure 3. a) Drain–source current (I_{ds}) versus drain–source voltage (V_{ds}) of WS_2 FET for various back gate bias voltage (V_{gs}) taken under vacuum. b) Transfer characteristics of WS_2 FET. c) Current–voltage (I_{ds}–V_{ds}) curve for Pedot:PSS connected in a FET configuration under vacuum with various back gate voltage biases ranging from −50 to +50 V. d) An optical image of actual Pedot:PSS/WS2 heterojunction device.

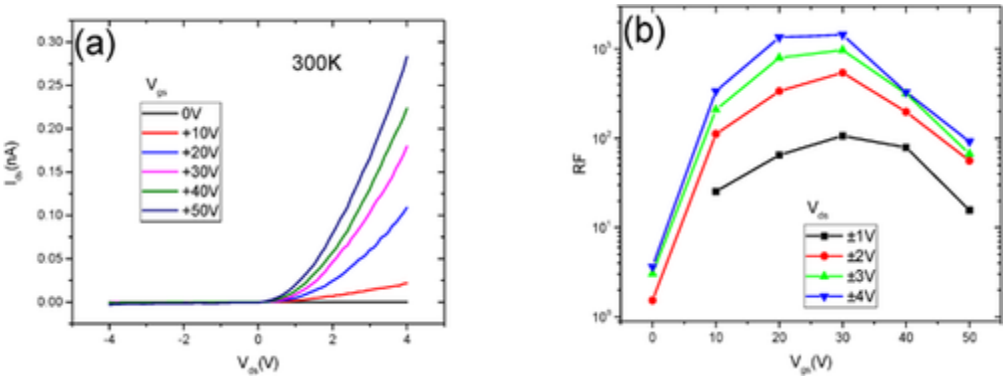

Figure 4. a) Drain current–voltage characteristics at various gate voltages in the dark and RT conditions. b) RF curves of Pedot:PSS/WS_2 device measured at different $\pm V_{ds}$ at various back-gate voltages.

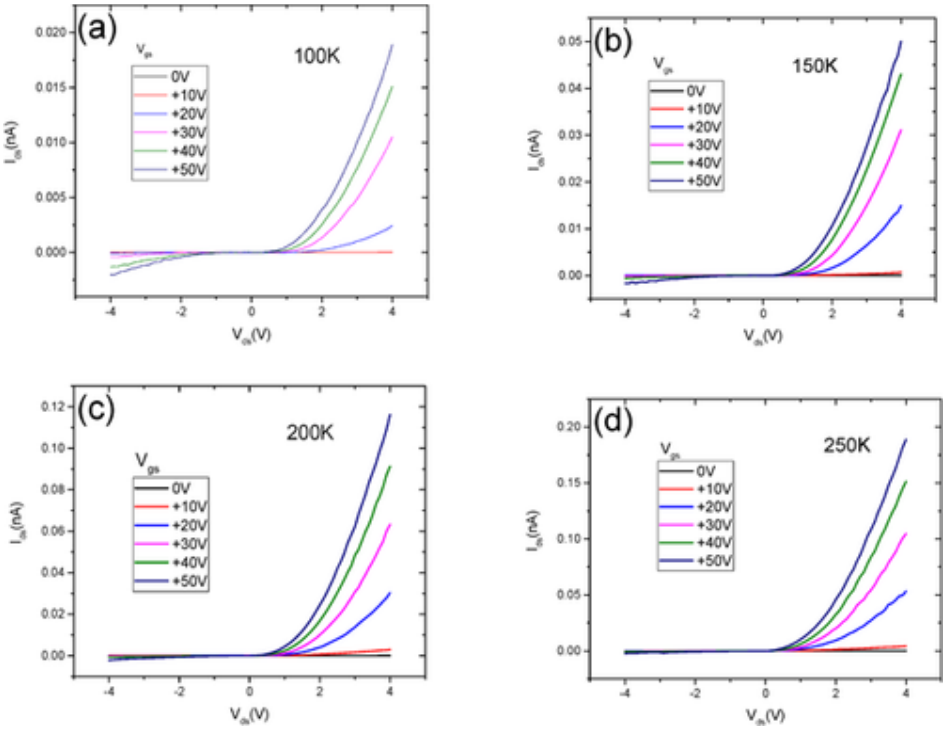

Figure 5. Drain current–voltage characteristics at various gate voltages at (a) 100, (b) 150, (c) 200, and (d) 250 K, respectively, in the dark condition.

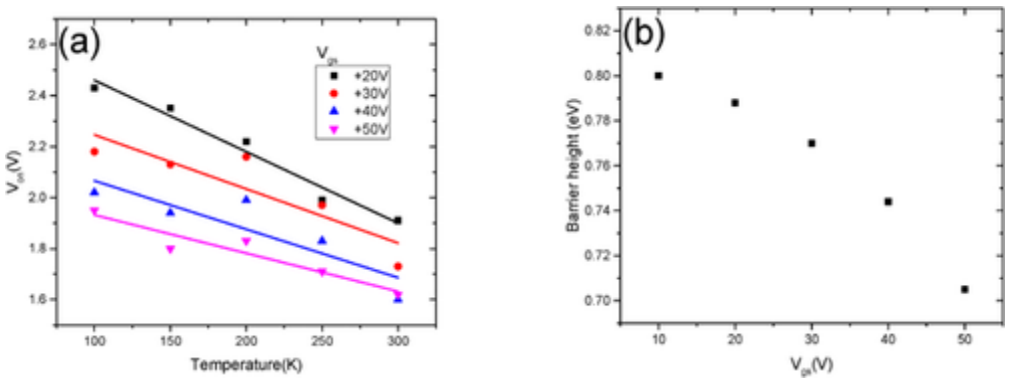

Figure 6. a) Turn on voltage of diode at various gate voltages from 100 to 300 K. b) The barrier height of Pedot:PSS/WS_2 heterojunction as a function of back-gate voltage bias.

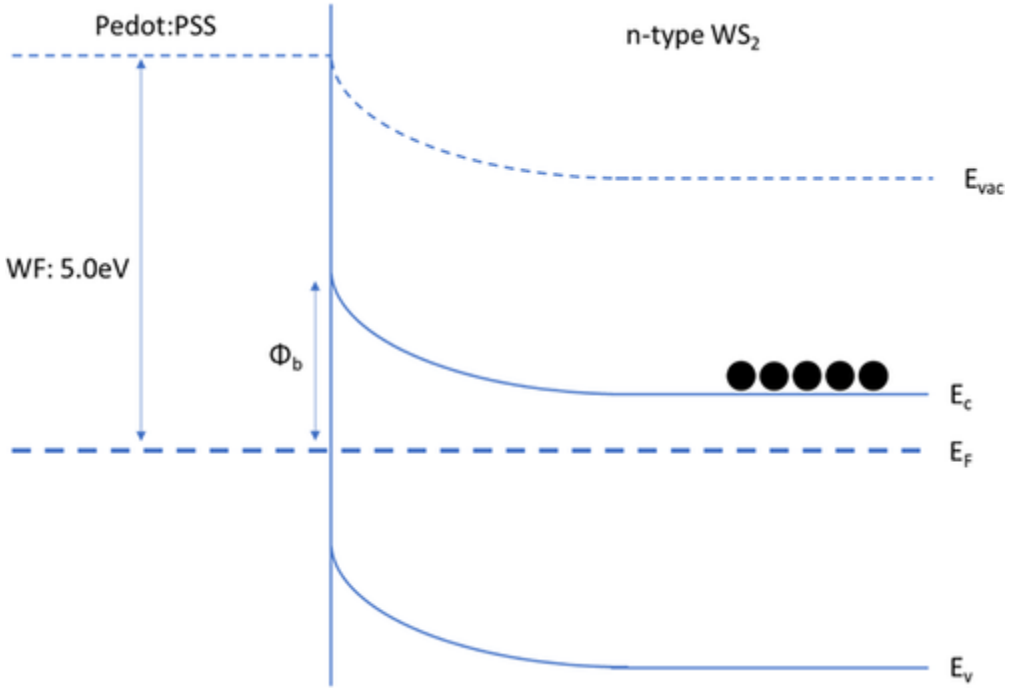

Figure 7. Schematic band diagram of the Pedot:PSS/WS_2 heterojunction.

Reference

[1] K. S. Novoselov, A. K. Geim, S. V. Morozov,D. Jiang, Y. Zhang, S. V. Dubonos, I. V. Grigorieva,A. A. Firsov,Science2004,306, 666.

[2] F. Schwierz,Nat. Nanotechnol.2010,5, 487.

[3] A. Gupta, T. Sakthivel, S. Seal,Prog. Mater. Sci.2015,73, 44.

[4] W. Choi, N. Choudhary, G. H. Han, J. Park, D. Akinwande, Y. H. Lee,Mater. Today2017,20, 116.

[5] S. C. Dhanabalan, J. S. Ponraj, H. Zhang, Q. Bao,Nanoscale2016,8,6410.

[6] J. S. Ponraj, Z. Q. Xu, S. C. Dhanabalan, H. Mu, Y. Wang, J. Yuan,P. Li, S. Thakur, M. Ashrafi, K. McCoubrey, Y. Zhang, S. Li, H. Zhang,Q. Bao,Nanotechnology2016,27, 462001.

[7] M. Xu, T. Liang, M. Shi, H. Chen,Chem. Rev.2013,113, 3766.

[8] A. Kuc, N. Zibouche, T. Heine,Phys. Rev. B2011,83, 245213.

[9] D. Ovchinnikov, A. Allain, Y.-S. Huang, D. Dumcenco, A. Kis,ACSNano2014,8, 8174.

[10] H. Bai, G. Shi,Sensors2007,7, 267.

[11] S. Kirchmeyer, K. Reuter,J. Mater. Chem.2005,15, 2077.

[12] F. Bonaccorso, A. Lombardo, T. Hasan, Z. Sun, L. Colombo,A. C. Ferrari,Mater. Today2012,15, 564.

[13] S. Zhang, Z. Yu, P. Li, B. Li, F. H. Isikgor, D. Du, K. Sun, Y. Xia,J. Ouyang,Organic Electron.2016,32, 149.

[14] A. Berkdemir, H. R. Gutierrez, A. R. Botello-Mendez, N. Perea-Lopez, A. L. Elías, C.-I. Chia, B. Wang, V. H. Crespi, F. Lopez-Urías, J.-C. Charlier, H. Terrones, M. Terrones,Sci. Rep.2013,3,1755.

[15] Z. Wang, X. He, X.-X. Zhang, H. N. Alshareef,Adv. Mater.2016,28,9133.

[16] F. Wang, Z. Wang, K. Xu, F. Wang, Q. Wang, Y. Huang, L. Yin, J. He,Nano Lett.2015,15, 7558.

[17] D. Jariwala, S. L. Howell, K.-S. Chen, J. Kang, V. K. Sangwan,S. A. Filippone, R. Turrisi, T. J. Marks, L. J. Lauhon, M. C. Hersam,Nano Lett.2016,16, 497.

[18] S. Velez, D. Ciudad, J. Island, M. Buscema, O. Txoperena, S. Parui,G. A. Steele, F. Casanova, H. S. van der Zant, A. Castellanos-Gomez,L. E. Hueso,Nanoscale2015,7, 15442.

[19] Y. Deng, Z. Luo, N. J. Conrad, H. Liu, Y. Gong, S.Najmaei, P. M. Ajayan, J. Lou, X. Xu, P. D. Ye,ACS Nano2014,8,8292.

[20] G. Horowitz,Adv. Mater.1990,2, 287.

[21] D. N. Ortiz, J. Vedrine, N. J. Pinto, C. H. Naylor, A. T. Charlie Johnson,Mater. Sci. Eng.: B2016,214, 68.

[22] M. K. Lee, S. M. Sze,Semiconductor Devices: Physics and Technology,3rd ed., International student ver. ed., Singapore, Wiley & SonsSingapore Pte. Ltd., Singapore2013